ACS OMEGA

http://pubs.acs.org/journal/acsodf

Article

Sustainable Approach of Using *Arundo donax* Leaves Reinforced Cement Mortar/Fly Bottom Ash Composites

Houda Hachem,* Insaf Mehrez, Ibtissem Boumnijel, Abdelmajid Jemni, and Daoued Mihoubi

Cite This: *ACS Omega* 2023, 8, 12039−12051

Read Online

ACCESS | Metrics & More | Article Recommendations

ABSTRACT: Earlier research suggested using ash to substitute cement, whereas other studies looked at the possibility of using plant-derived agricultural wastes as fiber reinforcement in cement applications. This study offered an environmentally friendly option to change traditional mortars by replacing cement with fly bottom ash (FBA) waste at 10, 20, 30, and 40 wt %. Likewise, *Arundo donax* leaves (ADL) were employed to reinforce the modified cement mortars at 0.4, 2, 5, and 7 wt %. X-ray diffraction analysis of used materials was performed. The morphology of composites made with FBA and ADL was investigated using scanning electron microscopy. Moreover, the density, water uptake, thermal conductivity, energy gain, and carbon dioxide (CO_2) emissions of the prepared composites were discussed. Their flexural strength, compressive strength, and displacement were also compared. Results revealed that the addition of FBA in the mortar matrix has a positive effect on decreasing the thermal conductivity and lightness of the mortar. In addition, 20 wt % of cement replacement by FBA guarantees simultaneously moderate mechanical properties, nearly 51% of energy gain, and 20% of total CO_2 emission reduction. In the same, adding ADL to the 20wt %FBA mortar reduced the thermal conductivity and the lightness of the mortar. The 0.4 wt % ADL reinforcement ensured 59% energy gain and 6% of total CO_2 emission reduction. A major amelioration was observed in the compressive strength (an increase of 14%) and in the plasticity (an increase of 27%) of the considered composite materials. In conclusion, using FBA as a cement replacement with low ADL content inclusion results in a thermal-resistant composite with reasonable durability and strength.

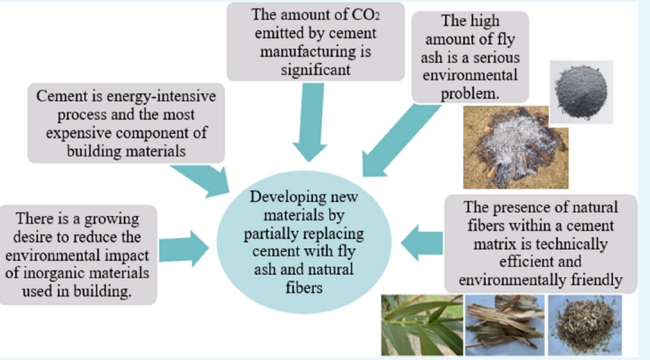

1. INTRODUCTION

Nowadays, a growing desire to minimize inorganic resources is deployed in buildings. Cement production is a high-energy process, and cement is the most expensive component among building materials. Added to that, the quantity of CO_2 produced by cement manufacturing is very significant.[1] Fly ash (FA) has been considered an unsafe solid waste.[2] The high amount of FA, derived from thermal power stations because of coal combustion, presents a serious environmental problem.[3] Thus, much research focuses on developing low-carbon materials by partly substituting cement with FA.[4] The use of FA mixed with other materials, in a range of applications, is an economical and environmentally friendly solution.[5,6] The optimal content of FA in cement composites can decrease production costs, reduce released CO_2 emissions, and conserve natural resources.[6] The FA cement composite has a variety of positive properties. It is significantly more solid and smooth.[7] Recently, Meng et al.[8] focused on the enhanced use of FA in cement composites. They found that coating TiO_2 nanoparticles on the surface of FA improves the interfacial interlocking between FA and cement and increases the early-age pozzolanic activity of FA.

da Luz Garcia and Sousa-Coutinho[9] focused on characterizing ground bottom ash (BA), with strength and durability assessment, as 5 and 10% cement replacement in mortars. They concluded that, when compared to the control mortar for ages up to 90 days, BA did not enhance the qualities of mortars. However, strength was nearly 12% higher in 1 year. Akinyemi and Dai[10] showed that the composition with the lowest cement content yielded a minimum thermal conductivity value of 0.62 W m^{-1} K^{-1} when compared with the thermal conductivity of concrete at around 1.91 W m^{-1} K^{-1}. According to Maschio et al.,[11] the highest amount of ash that can be utilized to replace cement is roughly 5 wt.%, and higher amounts do not produce appropriate physico-mechanical behaviors. According to Barbosa et al.,[12] the replacement of

Received: December 7, 2022
Accepted: March 10, 2023
Published: March 21, 2023

(a) (b) (c)

Figure 1. (a) Raw ADL plant, (b) dried ADL, and (c) crushed ADL.

Table 1. Mix Proportions of Cement Mortar Composites

sample designations	FBA content (wt %)	ADL content (wt %)	m_{cement} (kg)	m_{ash} (kg)	m_{sand} (kg)	m_{ADL} (kg)	[a] m_{water} (kg)
CM	0	0	0.240	0	0.403	0	0.144
CM/10FBA	10	0	0.216	0.024	0.403	0	0.130
CM/20FBA	20	0	0.192	0.048	0.403	0	0.115
CM/30FBA	30	0	0.168	0.072	0.403	0	0.101
CM/40FBA	40	0	0.144	0.096	0.403	0	0.608
20FBA/0.4ADL	20	0.4	0.222	0.044	0.373	0.003	0.133
20FBA/2ADL	20	2	0.218	0.043	0.367	0.013	0.131
20FBA/5ADL	20	5	0.212	0.042	0.356	0.032	0.127
20FBA/7ADL	20	7	0.207	0.041	0.348	0.045	0.124

[a] W/C = 0.6.

10% of the cement with FA has increased the compressive strength to a level that is comparable to that of the reference formulation. The new formulations showed chemical species emission levels that were comparable to, or even below, those seen for the reference formulation.

Using natural fibers as reinforcement in green cement and concrete applications increases the flexural strength, fracture toughness, and ductility of cement composites. Typically, this aims to create cheaper and environmentally safe building materials with enhanced strength properties.[13] Numerous research outputs have identified cellulosic fiber-reinforced cement matrices[14] like jute, hamp, sisal, malva, coconut, palm, banana, jute, bagasse, etc. as potential sources of nonconventional cement-mixed composite materials. In comparison to synthetic fibers, natural fiber particles have good mechanical qualities and are completely biodegradable.[15] *Arundo Donax*, known as giant reed, is a tall cane with a diameter of 20−30 cm[16] that grows widely and quickly in many places. *Arundo donax* is a common plant with a strong potential as a long-term structural plant. Many authors focus on using *Arundo donax* leaves in the building sector[17,18] mainly to obtain particleboards[19−21] and concrete block[16,22−24] or epoxy resin[15] reinforcement.

Shon et al.[23] found that when ADL fibers were mixed with cement mortars, the thermal conductivity and density of the concrete diminished. Manniello et al.[24] tested the tensile strength of cylindrical concrete blocks at a constant amount of ADL fibers (1 wt %) and different aspect ratios of 30, 50, and 70 (mm/mm). They found that larger aspect ratios generate better tensile qualities of concrete composites. Molari et al.[16] demonstrated that *Arundo donax* has mechanical properties like several bamboo species utilized in construction.

Several studies have been published to examine the use of FA as a construction material. Generally, the use of fly bottom ash (FBA), obtained from wood incineration, has not received much attention. The primary goal of this study was to focus on characterizing the used FBA and to examine how FBA affects mortar microstructure as well as thermo-physical and mechanical properties. The second purpose is to assess the ADL fiber loading effect on the mechanical and thermal properties of FBA mortar composites. Materials used to make composites were first characterized. The proposed composites were prepared and next put to the test in an experimental setting. By demonstrating the material's potential through rigorous thermal and mechanical evaluation, the acquired results stimulate the use of FBA and ADL natural fibers in engineering building practices.

2. MATERIALS AND METHODS

2.1. Materials. The studied composite samples were made with cement, sand, FBA, and *Arundo donax* leaves (ADL). The mortar was prepared from the Portland cement CEMII/A-L32.5R mixed with sand having a maximum granulometry distribution of 1 mm. The used FBA was collected from coal combustion in a traditional oven. Prior to its use, the collected FBA was sieved to remove impurities and large sand particles. As demonstrated in the sieve analysis part of FBA (3.1.2), the maximum size was about 1 mm. The *Arundo donax* leaves were collected from a Tunisian forest. The ADLs were dried first in the sun for 30 days and further in an oven at 50 °C until reaching a dry state. Afterward, ADLs were crushed mechanically to extract fibers with lengths ranging from 0.5 to 3 mm, as revealed in the sieve analysis part of ADL (4.2.2). The dried and crushed ADLs were then used for preparing the composites (Figure 1).

2.2. Composite Preparation. All mortars were prepared based on cement, sand, and water. Tap water with pH = 7.5 was used for mixing the samples. The reference mortar sample denoted as CM was made by combining sand with cement in a weight ratio of 2.0. All samples were prepared using a weight ratio of 0.6 (g water /g cement). Four FBA weight fractions of 10, 20, 30, and 40% were mixed to cement mortar CM. Composites are prepared, manually using a traditional procedure (hand mixing), and labeled CM/10FBA, CM/20FBA, CM/30FB, and CM/40FBA, respectively. The homogenized mixture was manually poured into a parallele-

https://doi.org/10.1021/acsomega.2c07818
ACS Omega 2023, 8, 12039−12051

piped mold. For that, two types of molds with dimensions of 27 × 27 × 4 and 16 × 4 × 4 cm^3 were manufactured for thermal and mechanical tests, respectively.

Four ADL weight fractions of 0.4, 2, 5, and 7% were mixed to CM/20FBA. Composites are prepared and labeled 20FBA/0.4ADL, 20FBA/2ADL, 20FBA/5ADL, and 20FBA/7ADL, respectively. Mix proportions of all cement mortar composites are shown in Table 1. A repeated technique was utilized while preparing composites according to the standard ASTM D790.[37] To guarantee homogeneity, all components were properly blended for 2 min before and after adding water. All the specimens were removed from the mold after 24 h and conserved for 28 days under laboratory conditions.

2.3. Methods. *2.3.1. X-ray Diffraction Analysis.* Using a D8 Bruker advance diffractometer, XRD analysis was performed to determine the composition of the employed cement, sand, FBA, and ADLs. Various components were scanned using Cu-K radiation at 40 KV and 40 mA with a step size of 0.02° in the 2θ range from 10 to 50° at room temperature. Following the Segal empirical approach,[25] the crystallinity index (CI) of ADL was calculated as follows:

$$\mathrm{CI}(\%) = \left[\frac{I_{22^\circ} - I_{18^\circ}}{I_{22^\circ}}\right] \times 100 \tag{1}$$

2.3.2. Microscopic Observation. FBA and ADL were observed using two digital processing units: a binocular magnifier of type Zeiss Stemi 2000-C Stereo (zoom range: 6.5×−50×) and an optical microscope of type Axioskop 40 (zoom range: 200/0.45, Infinity/0.17). For image observation, the samples have been uniformly distributed on a microscope slide.

2.3.3. Scanning Electron Microscopy. The morphology of the used ADLs and the surfaces of composites were examined using scanning electron microscopy (SEM) ZEIXX field emission. Silver plates were used to fix samples. In a vacuum chamber, they were covered with a small layer of gold to make them conductors and ensure a good observation.

2.3.4. Water Uptake Determination. The proposed composite was first heated in an oven set to 50 °C until its mass became constant, noted w_0. Afterward, composites were immersed in a water container. After 3 days, each composite sample was weighted and noted w_t. Finally, the water uptake (W_a) was determined as follows:[26]

$$W_a = \frac{w_t - w_0}{w_0} \times 100 \tag{2}$$

2.3.5. Thermal Conductivity Measurement. The hot box method was used to assess thermal conductivity. The composite sample was placed between a heated, at T_h, and a cooled, at T_c, source to generate a unidirectional temperature gradient. More details about the experimental setup were shown in the previous work of Mehrez et al.[26] The thermal conductivity (k) was calculated as follows:

$$k = \frac{e}{S(T_h - T_c)}\left(\frac{U^2}{R} - \beta(T_b - T_a)\right) \tag{3}$$

where $\Delta T = T_h - T_c$, $\Delta T' = T_b - T_a < 1°C$, $\beta = 0.16\ \mathrm{W\ K^{-1}}$, $R = 5000\ \Omega$, $0 < U < 220$ V.

It is worth noting that different thermal conductivity measurement techniques and scientific standards of different cement-based materials used in previous studies were reviewed by Asadi et al.[27]

2.3.6. Energy Gain Determination. The energy gain can be calculated as the ratio of the proposed composite heat flux and those of the reference mortar. Assuming that the two samples have the same thickness and are exposed to the same temperature gradient, the energy gain (Eg) can be assessed as the ratio of their thermal conductivities (eq 4).:[28]

$$\mathrm{Eg} = 100 \times \left(1 - \frac{k_{comp}}{k_{ref}}\right) \tag{4}$$

where k_{ref} is the thermal conductivity of the reference mortar and k_{comp} is the thermal conductivity of the composite sample.

2.3.7. Carbon Dioxide Emissions. The effect of incorporating FBA and/or ADL in the cement matrix on CO_2 emissions was investigated. The primary causes of CO_2 emissions include the emitted CO_2 from calcination ($CO_{2calcination}$), the emitted CO_2 from the thermal energy used in cement production ($CO_{2thermal\ energy\ use}$), and the CO_2 emissions associated with cement and clinker transportation at a certain distance by a certain mode[29] ($CO_{2transportation}$). The total amount of emitted CO_2 can be calculated as follows:

$$\begin{aligned}\text{total } CO_{2\,\mathrm{Emissions}} &= CO_{2\,\mathrm{calcination}} + CO_{2\,\mathrm{thermal\ energy\ use}} \\ &\quad + CO_{2\,\mathrm{transportation}} \\ &= m_c \cdot p_{\mathrm{clinker}} \cdot 0.51 + V_{\mathrm{fuel}} \cdot \rho_{\mathrm{fuel}} \cdot U_{CO_2} \\ &\quad + m_c \cdot d \cdot \mathrm{ft}\end{aligned} \tag{5}$$

The main simplifying assumptions are that energy consumption is 1 L of diesel oil or 1 kg of coal, the transportation distance is about 10 km, and the mode of transport is considered as rail, electric, and diesel. More details were given in the previous work of Pommer and Pade.[30]

2.3.8. Mechanical Strength Determination. For all tests, the standard EN 196-1 was used to determine flexural and compressive strengths. The mechanical measurements were carried out, at an age of 28 days, using the LLYOD machine which has a load capacity of 20 KN. For flexural and compressive tests, the load speed velocity was set to 10 and 5 mm/min, respectively. The applied load according to displacement was recorded by the machine software acquisition. The flexural strength R_f (6) and compressive strength R_c (7) were calculated considering three replicate measurements and expressed as follows:

$$R_f = \frac{3Fl}{2bh^2} \tag{6}$$

$$R_c = \frac{F}{A} \tag{7}$$

where F is the average applied force to a cross-section, b is the width of the test sample, h is the thickness of the test sample in the direction of bending, l is the support span (0.1 m), and A is the across a section.

3. RESULTS AND DISCUSSION

3.1. Effect of FBA Replacement in the Cement Mortar. *3.1.1. Morphology of FBA.* Microscopic observation of the used ash was performed. Images show that the particle size distribution of the used ash powder is inhomogeneous.

https://doi.org/10.1021/acsomega.2c07818
ACS Omega 2023, 8, 12039−12051

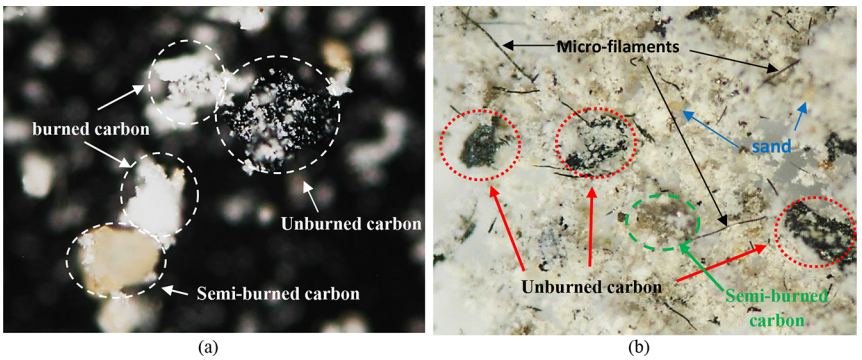

Figure 2. Fly and bottom ash viewed using (a) microscope (×200) and (b) binocular magnifier (×50).

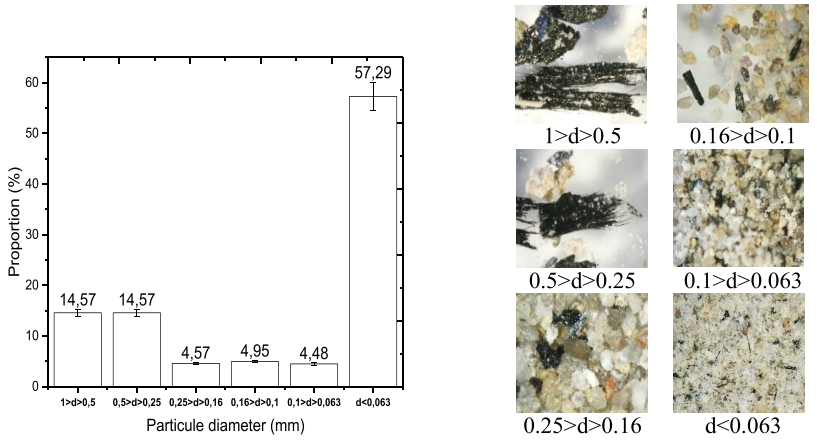

Figure 3. Sieve analysis grading curve and binocular magnifier view (×50) of used FBA.

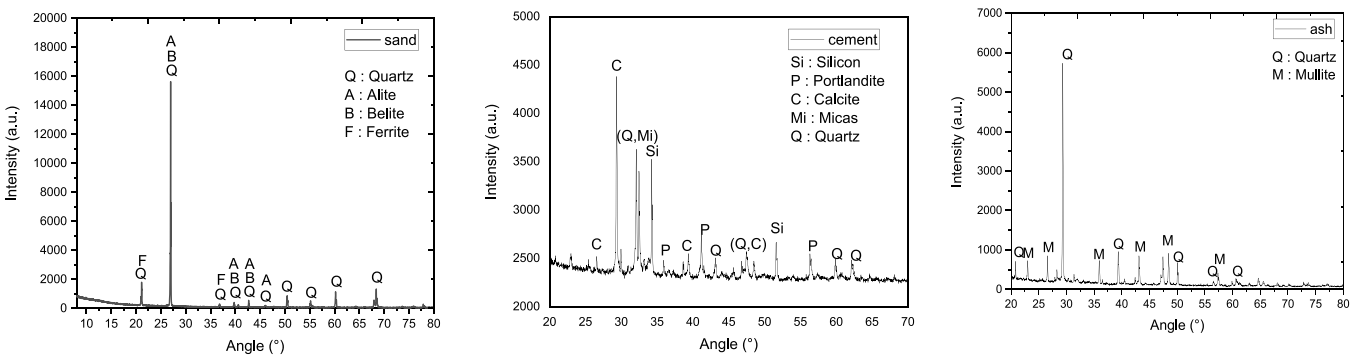

Figure 4. XRD patterns of (a) sand, (b) cement, and (c) FBA.

Observations using a microscope (Figure 2a) and binocular magnifier (Figure 2b) show particles of different sizes, colors, and geometries. The microfilaments and the large black particles represent the noninflamed carbon whereas the yellow particles are the semi-burned carbon which are BA. The white color particles of spherical shape are the FA. Other impurities like sand are also present. Thus, the used ash powder is composed of FA mixed with inhomogeneous BA particles and a few sand particles. As a result, the inhomogeneity of the used FBA increases the porosity of the prepared cement mortar.

3.1.2. Seive Analysis of FBA. Figure 3 shows the grading curves of the FBA used in preparing samples and their binocular magnifier views at various granulometric levels. About 57% of ash particle diameter is less than 0.063 mm which represents nearly the amount of FA. The remaining 43% is composed of unburned carbon that has been combined with sand particles.

3.1.3. X-ray Diffraction of Sand, Cement, and FBA. The XRD patterns of the used sand, cement, and FBA are represented in Figure 4a−c, respectively. The main components of sand are quartz (SiO_2), alite (Ca_3SiO_5), belite (Ca_2SiO_4), and ferrite labeled by *Q*, *A*, *B*, and *F*, respectively.[31]

The main components of the cement sample are silicon (Si), portlandite ($Ca(OH)_2$), calcite ($CaCO_3$), mica $[(Si,Al)_2O_5]_n$, and quartz (SiO_2) (Figure 4b). These components will react in the cement hydration process to strengthen its structure. On the other hand, the major components identified in the FBA structure are quartz (SiO_2) and mullite ($Al_6Si_2O_{13}$) which are

https://doi.org/10.1021/acsomega.2c07818
ACS Omega 2023, 8, 12039−12051

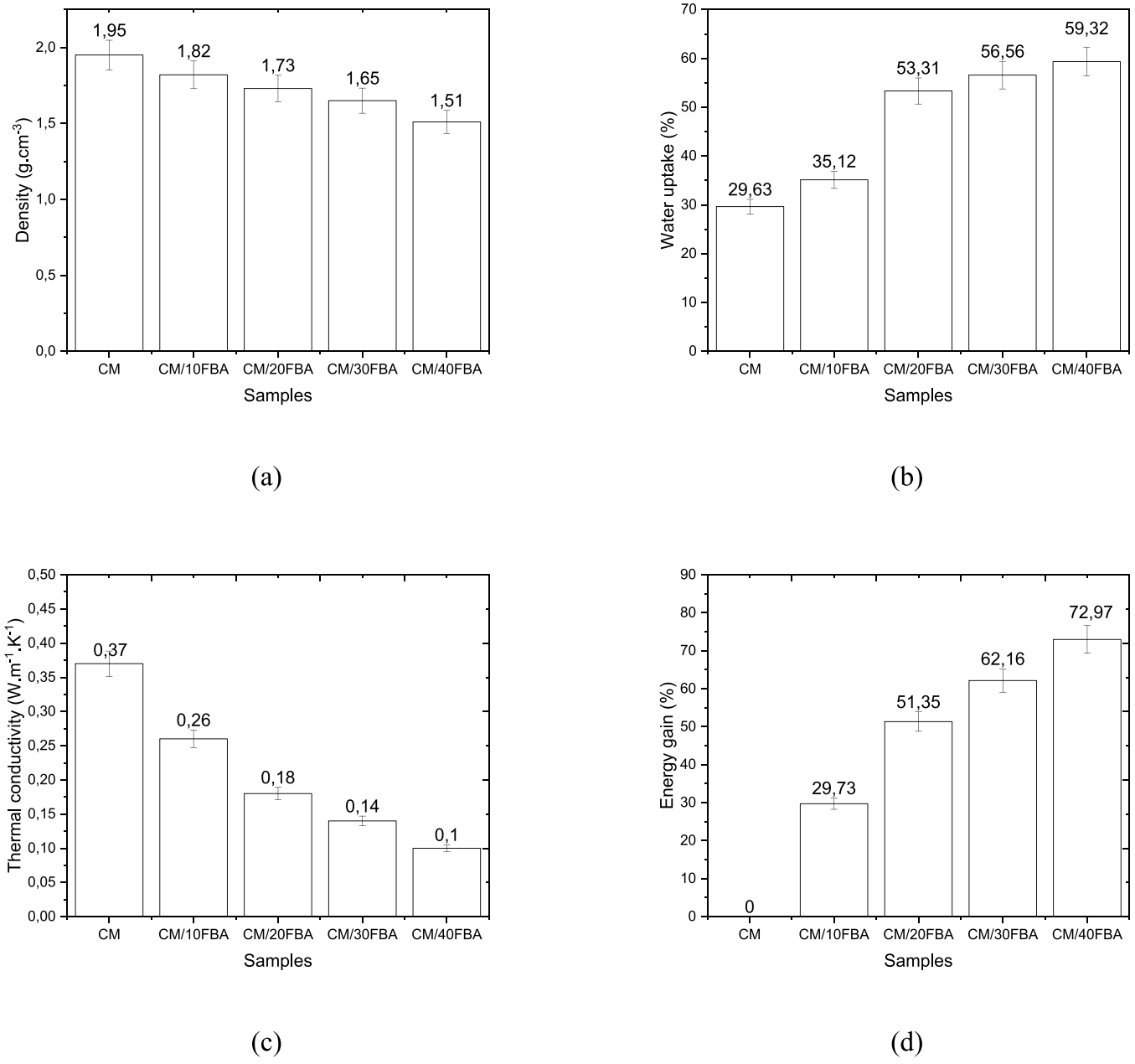

Figure 5. Effect of FBA replacement in the cement mortar on (a) density, (b) water uptake, (c) thermal conductivity, and (d) energy gain.

able to increase the strength and improve the durability of composites.

3.1.4. Thermo-Physical Properties and Energy Gain of FBA Composites. Experiments were carried out to assess the impact of cement replacement by FBA at different contents on density, water uptake, thermal conductivity, and energy gain of CM/FBA composites.

As seen in Figure 5a, the composite density decreases with the increase in FBA content. The highest density decrease is about 22% using CM/40FBA. All CM/FBA composites become more lightweight compared to the reference mortar which is an interesting and promising characteristic of these composites.

The water uptake test of each CM/FBA composite was investigated, and the obtained results are illustrated in Figure 5b. According to this figure, water uptake increases with FBA content. This behavior contributes to the deterioration of building materials like the mortar and concrete[32] possibly caused by the occurrence of hydrophilic groups including (OH) groups, frequently available in the FBA material.[55]

The thermal conductivities measured after 28 days (Figure 5c) of the prepared samples were also assessed. Replacement of the cement mortar by FBA inside the composite leads to a thermal conductivity decrease. This can be explained by the fact that air voids inside the composite increase due to the decrease of density.[33] The same findings were reported by Caprai et al.[34] during his study on heat conductivity in blended cement. He demonstrated that thermal conductivity decreased from 0.75 to 0.4 W m^{-1} K^{-1} when BA is used to replace 50% of the cement paste. Similar observations were discovered by Demirbog[35,36] where he showed that lower thermal conductivity levels were obtained when the overall porosity increased due to the ash content increase.

https://doi.org/10.1021/acsomega.2c07818
ACS Omega 2023, 8, 12039−12051

Table 2. CO_2 Emissions from Different CM/FBA Composites

sample	cement content	$CO_{2calcination}$	$CO_{2thermal\ energy\ use}$	$CO_{2transportation}$	CO_{2tot}
CM	0.240	0.098	1.152	0.072	1.321
CM/10FBA	0.216	0.088	1.152	0.065	1.240
CM/20FBA	0.192	0.078	1.152	0.058	1.230
CM/30FBA	0.168	0.069	1.152	0.050	1.220
CM/40FBA	0.144	0.059	1.152	0.043	1.211

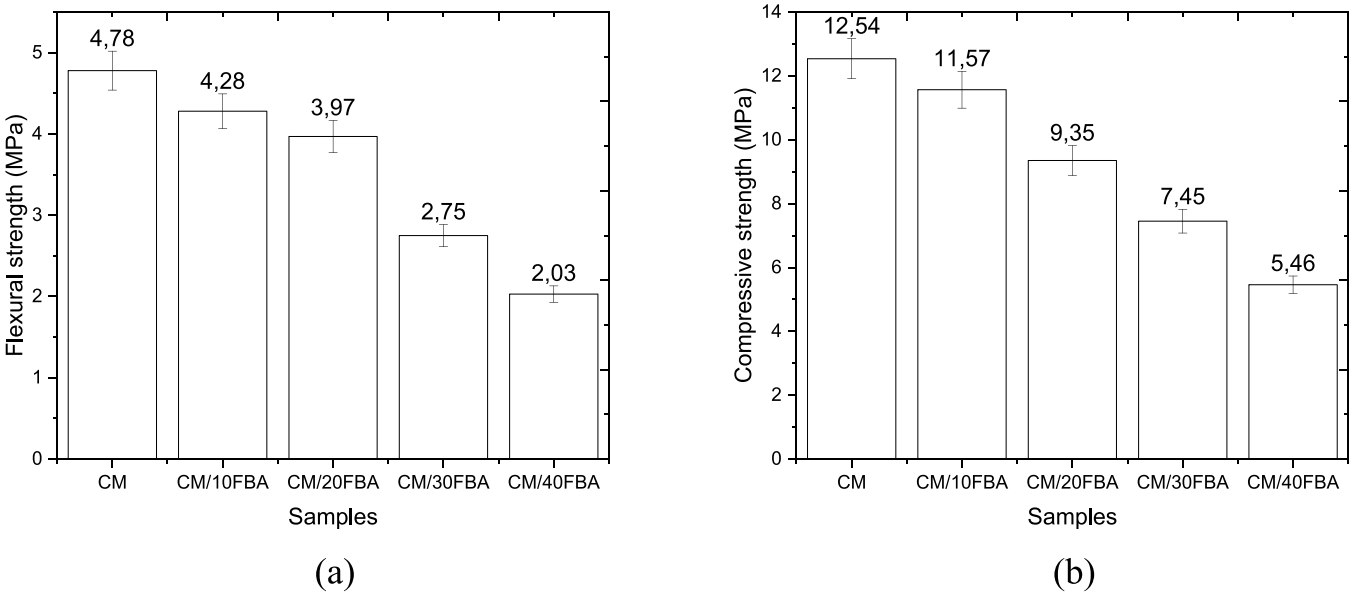

Figure 6. Effect of FBA content on (a) flexural and (b) compressive strengths according to the ISO-standard after 28 days.

Energy gain values, calculated using eq 4, are presented in Figure 5d. The use of CM/40FBA composite guarantees almost 73% energy gain. Accordingly, the cement mortar replacement by FBA represents a promising solution to reduce energy consumption in the building.

3.1.5. Environnemental Impact of FBA Composites. The pollution potential of the composites prepared by partially substituting cement with FBA was assessed. CO_2 emissions were calculated using eq 5, and the obtained results are gathered in Table 2. As seen in this table, the total CO_2 emissions decrease with regard to the reference mortar (CM) which can be attributed to the reduction of cement content in the proposed composites after the partial replacement with FBA. From an environmental point of view, this latter finding highlights the benefits of incorporating FBA into mortar preparation.

Nevertheless, it is worth noting that in the present study, it is assumed that the calcination, manufacture, and transportation of cement and clinker were the most major critical effects on CO_2 emissions from the proposed construction materials considering the fact that FBA is seen as a waste that is already generated and available. Accordingly, the contribution of FBA production to CO_2 emissions was not considered. The same predictive carbon dioxide emission model was adopted by Dodoo et al.[46] in 2009 and recently by Ibeto et al.[47] in 2020. According to Dodoo et al.,[46] a building with a wood frame emits much fewer carbon emissions than one with a concrete structure. On the other side, Ibeto et al.[47] showed that adding coal ash to cement reduced emissions by 0.22−0.33 kg when cement and sand were replaced by 10−40% coal ash without including the contributions of FBA in CO_2 emissions.

3.1.6. Mechanical Properties. According to ASTM D790-10,[37] flexural and compressive tests of all composite samples were performed, and results are presented in Figure 6a,b, respectively. Samples of 16 × 16 × 4 cm^3 were used for flexural tests. Three samples are evaluated for each case. The six halves of the sample recovered after rupture in the flexural test were employed in the compressive test. Results reveal that flexural and compressive strengths decrease with FBA content due to the high porosity of the mixture. The resistance of the used CM is about 5 and 12 MPa, respectively, at the flexural and compressive tests wherein values are nearly like those obtained by Saghrouni et al.[38] and Mehrez et al.[45] Figure 7 shows the load−displacement curves of the composites. The reference mortar presents a sudden rupture at 0.42 mm. Whatever the FBA content, the rupture behavior is conserved but the displacement has been changed. The CM/40FBA composite has the highest displacement value (0.47 mm) compared to that of the reference (CM).

The sample CM/20FBA is retained for the rest of the experiments given that the use of CM/20FBA guarantees an energy gain of about 51% and did not strongly affect mechanical strengths. Likewise, using CM/20FBA, the flexural and compressive strengths and displacement slightly decrease by 0.8 MPa, 3.19 MPa, and 0.01 mm, respectively, with regard to the reference mortar CM. Antiohos et al.[39] validated this findings; they demonstrated that the mixture was best efficient for a modest cement substitution (20 wt %), whereas the mechanical resistance was reduced for greater FBA replacements (30 wt %). Many phenomena are at the origin of this behavior including the damping of vibrations and adding to the disorder of the overall matrix. The findings of Song et al.[54] may

https://doi.org/10.1021/acsomega.2c07818
ACS Omega 2023, 8, 12039−12051

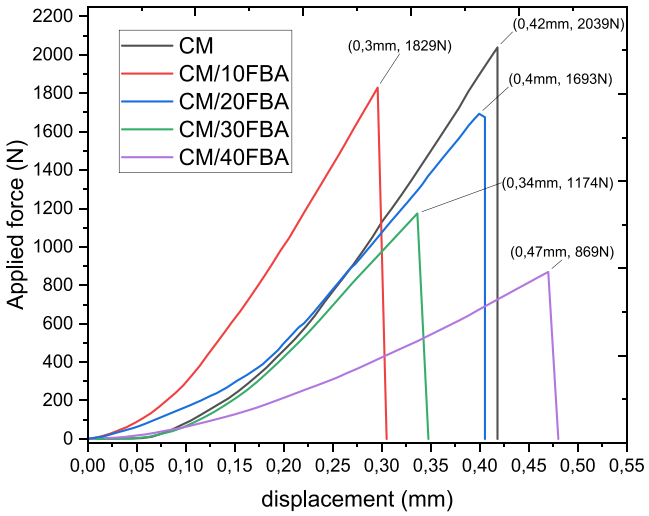

Figure 7. Load−displacement curves from the flexural test of CM/FBA composites according to the ISO-standard after 28 days.

assist in the development of nanoscopic techniques to enhance cement and its eventual qualities.

3.1.7. Morphology of the FBA Composite. Figure 8 depicts SEM micrographs of the CM/20FBA composite at three distinct enlargements of 500, 100, and 50 μm. Pictures were obtained from the fractured surface (after the flexural mechanical test) of the CM/20FBA composite sample to examine the bonding of FBA to the cement mortar. Compared to the standard cement mortar, the structure of the CM/20FBA composite appears to be very different. More porous microstructure can be clearly seen with the incorporation of FBA in the cementitious mortar matrix. FA has a regular morphology of very small spherical particles as previously reported in the research of Kosmatka et al.[40] Nevertheless, BA has an irregular morphology where BA particles have distinct forms and different sizes with irregular morphology. They appear very porous like a honeycomb structure, resulting in increasing air voids inside the composite structure and decreasing density. This morphology confirms the experimental results presented in the previous section in relation to lightness and low thermal conductivity values of the prepared composites made with FBA. Considering the forgoing discussion, CM/20FBA will be the retained composite, in the rest of the article, to be reinforced with natural ADL fibers.

3.2. Effect of Natural ADL Fiber Inclusion. Natural fibers from *Arundo donax* leaves (ADLs) were characterized using the same methods.

3.2.1. Morphology of ADL. Figure 9 presents SEM micrographs of ADL at three distinct enlargements of 500, 100, and 50 μm. Images show that ADL fibers are covered with a very thin vegetable layer below which very thin empty tubes bonded to each other. The ADL fiber morphology is made up of an irregular tube size. Like major natural fibers, the ADL fibers' surface morphology is formed of several elementary fibers that are joined together throughout their length by pectin and other noncellulosic substances.[41] Likewise, the fiber surface clearly shows some impurities. In fact, natural fibers are frequently subjected to chemical treatments to remove these impurities and improve their interfacial adhesion with a cement matrix.[42]

3.2.2. Sieve Analysis of ADL. Figure 10 shows the grading curves for the used ADL fibers to prepare samples as well as their binocular magnifier views at various granulometric levels (magnification of 20 or 50 times). As seen in this figure, almost 55% of ADL particles diameter is higher than 2 mm.

3.2.3. X-ray Diffraction Characterization of ADL. The XRD pattern of the used ADL, shown in Figure 11, presents an intense peak located at $2\theta = 22.5°$ (101) and a slight peak at $2\theta = 16°$ (110) corresponding to crystalline planes. The calculated CI value of ADL, using eq 1, is about 54% which is completely in agreement with data already reported in the literature for this kind of biomass.[43]

3.2.4. Thermo-Physical Properties and Energy Gain of FBA/ADL Composites. Given that CM/20FBA was the retained composite; it is then reinforced with ADL fibers to ameliorate its properties. The effect of ADL loading on density, water uptake, thermal conductivity, and energy gain is reported in Figure 12. The ADL content ranged between 0.4 and 7% of the mass fraction.

The density decreases with increasing the ADL content (Figure12a). This result can be justified by the low density of ADL reported to be 0.893 g cm^{-3}.[44]

The water uptake is inversely proportional to the composite density evolution but increases with ADL content (Figure 12b). The strong capacity of ADL fibers to absorb water accounts for this behavior. The 20FBA/0.4ADL composite has the lowest water uptake (reduction of 21%), which is a desirable character for construction composites. Moreover, it can be noticed that the thermal conductivity of composites

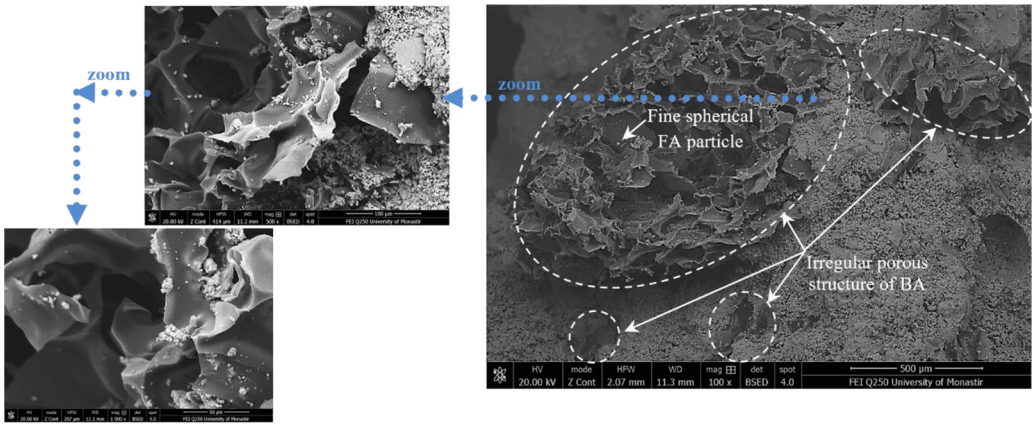

Figure 8. SEM images of the CM/20FBA composite at 500,100, and 50 μm.

https://doi.org/10.1021/acsomega.2c07818
ACS Omega 2023, 8, 12039−12051

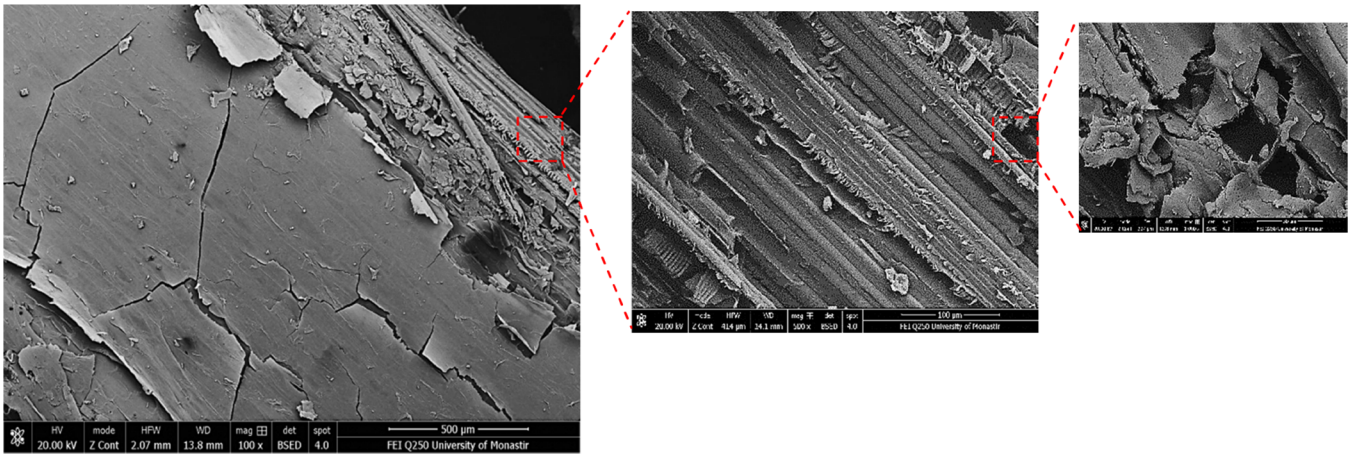

Figure 9. SEM images of ADL fibers at different magnifications (500,100, and 50 μm).

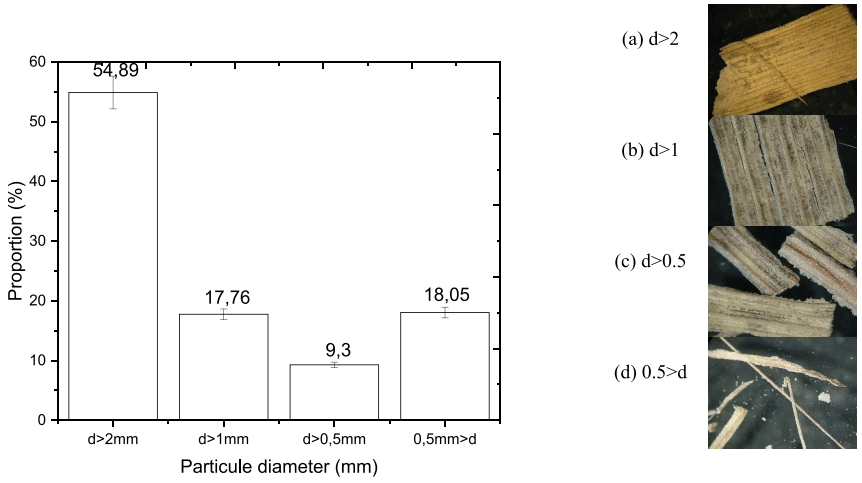

Figure 10. Sieve analysis grading curve and binocular magnifier views (a) ×20 and (b–d) ×50 of the used ADL fibers.

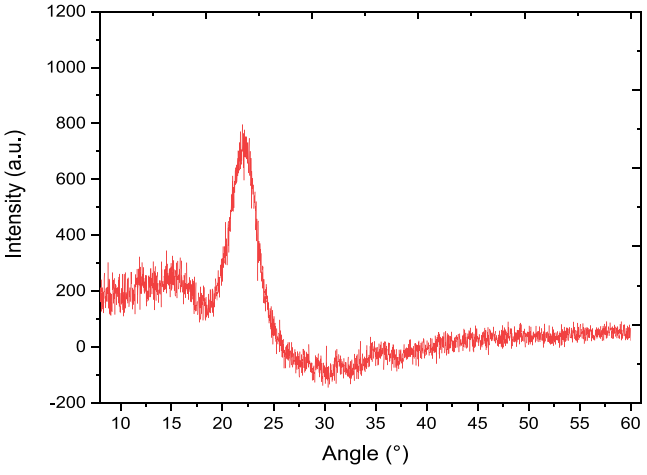

Figure 11. XRD pattern of the used ADL fibers.

decreases with the ADL content (Figure 12c). As these short fibers are added to the mortar matrix, the amount of air voids in the materials increases leading to porosity rise. Nevertheless, the increase of ADL content causes a decrease in thermal conductivity nearly from 0.15 to 0.09 W m^{-1} K^{-1} resulting in a maximum energy saving of about 76% when using 7 wt % of ADL reinforcement. On the other hand, a 0.4 wt % ADL composite, having lower moisture properties, results in an energy saving of about 59.5% as shown in Figure 12d.

The same observations were approved by Hamdaoui et al.[48] and Mehrez et al.[42] According to Hamdaoui et al.,[48] the addition of 20% of *Posidonia Oceanica* fibers reduced thermal conductivity by around 22% (from 0.0718 to 0.0559 W m^{-1} K^{-1}) compared to the reference cement matrix. According to Mehrez et al.,[42] the incorporation of wood aggregates into plaster increased thermal resistance (the thermal conductivity decreased from 0.27 to 0.141 W m^{-1} K^{-1}).

3.2.5. Environnemental Impact of FBA/ADL Composites. Composites prepared by partially replacing the mortar with ADL fibers were evaluated for their ability to cause pollution. In fact, after being partially replaced with ADL, cement content in the suggested composites decreased. Consequently, less CO_2 is released as shown in Table 3.

3.2.6. Mechanical Properties of FBA/ADL Composites. Figure 13a,b presents the flexural and compressive strengths of composites made with ADL fibers. The flexural and compressive strengths of 20FBA/0.4ADL respect almost the same order of magnitude as CM/20FBA strengths but they are still less than that of the cement mortar CM. Compared to the CM/20FBA composite, the slight increase of the compressive strength in 20FBA/0.4ADL can be attributed to the higher content of cement in 20FBA/0.4ADL as reported in Table 1. Nevertheless, the flexural and compressive strengths decrease

https://doi.org/10.1021/acsomega.2c07818
ACS Omega 2023, 8, 12039−12051

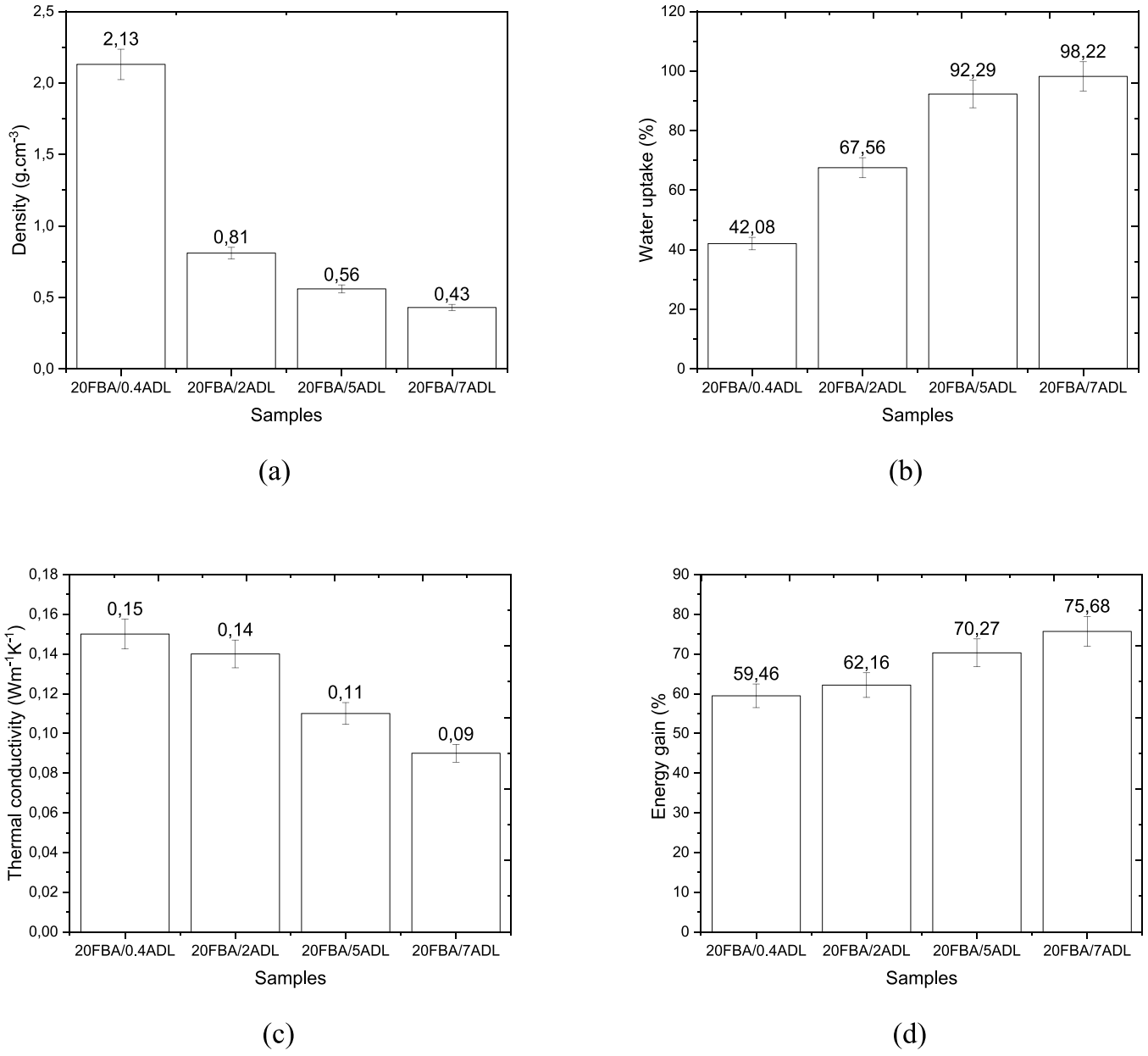

Figure 12. Effect of ADL loading on (a) density, (b) water uptake, (c) thermal conductivity, and (d) energy gain of the proposed composites.

Table 3. Predictive CO_2 Emissions from Samples Reinforced with ADL

sample	cement content	$CO_{2calcination}$	$CO_{2thermal\ energy\ use}$	$CO_{2transportation}$	CO_{2tot}
20FBA/0.4ADL	0.222	0.091	1.152	0.067	1.309
20FBA/2ADL	0.218	0.089	1.152	0.065	1.306
20FBA/5ADL	0.212	0.086	1.152	0.064	1.874
20FBA/7ADL	0.207	0.084	1.152	0.062	1.857

with increasing ADL content. This was also reported by some previous studies that focused on the combination of cement mortar and natural fibers.[42] In fact, the negative effect of ADL addition on the flexural and compressive strengths is due to the increase of the material porosity and the weak bond between ADL and CM/20FBA.

Figure 14 shows applied load−displacement curves for CM/20FBA reinforced with different ADL contents. The results reveal that the reference mortar (CM/20FBA without ADL fibers) has a brutal rupture with a displacement of 0.4 mm. The curve shape for the composite 20FBA/0.4ADL is similar to that for CM/20FBA whereas higher ADL content considerably decreases the applied load until the rupture. The nonlinear part of the curve is due to an elasto-visco-plastic deformation of the ADL fibers.

3.2.7. Morphology of the FBA/ADL Composite. Figure 15 shows SEM micrographs of the 20FBA/0.4ADL composite at two different magnifications of 100 and 50 μm. To analyze the bonding of the ADL to the mortar, SEM images were taken from the cracked surface of the 20FBA/0.4ADL composite

https://doi.org/10.1021/acsomega.2c07818
ACS Omega 2023, 8, 12039−12051

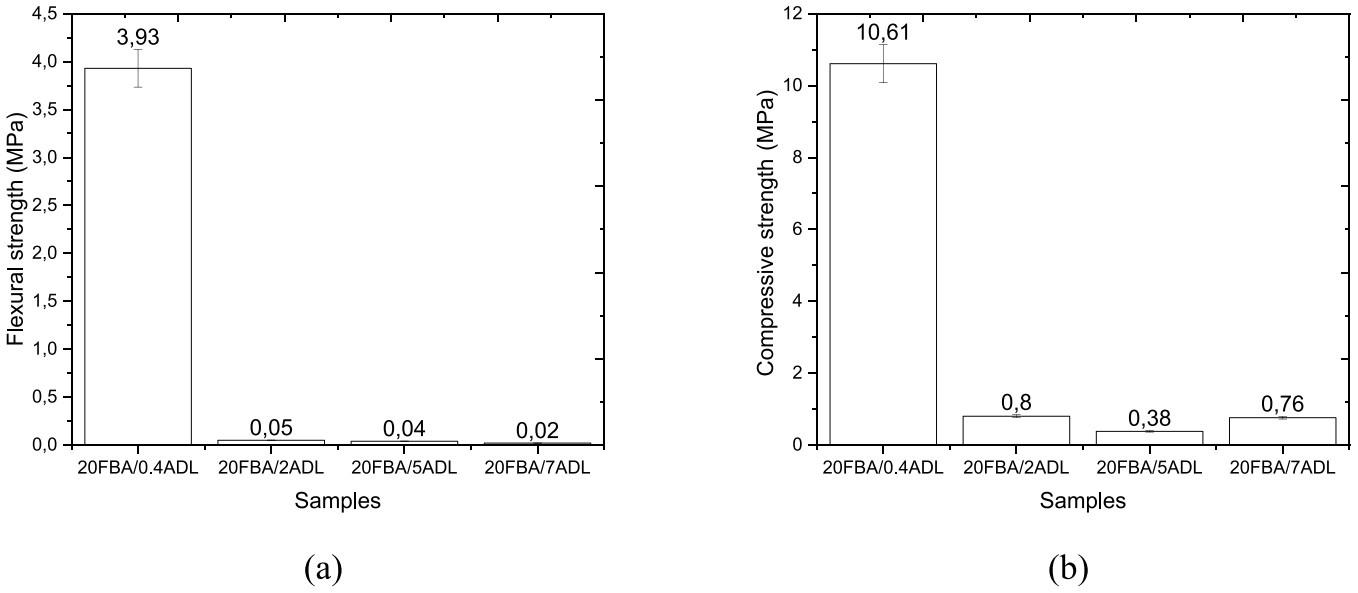

Figure 13. Effect of the ADL fiber ratio on the (a) flexural and (b) compression strengths according to the ISO-standard after 28 days.

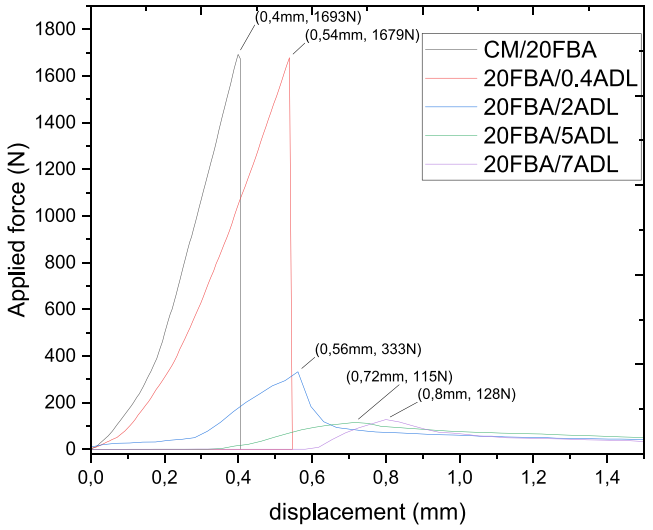

Figure 14. Load−displacement curves from the flexural test of samples reinforced with ADL fibers according to the ISO-standard after 28 days.

sample after the flexural mechanical test. It can be seen from the cross-section of the sample that there is no chemical reaction between the ADL and the mortar. Additionally, there are some holes that have appeared as a result of pulling off the ADL fibers. This phenomenon can be explained by the incompatibility of the mortar with the impure surface of the ADL fibers. As a result, the mechanical strengths of composites may be severely reduced at higher ADL content.

Overall, the utilization of some natural fibers such as hemp,[49] flax,[50] bagasse,[51] coconut,[52] sisal,[53] etc. can boost the mechanical strength of a weak matrix. However, the characteristics of cement reinforced with natural fibers can be influenced by a number of factors such as fiber type, geometry, surface area, matrix quality, mixing process, drying method, etc. In the present paper, the utilization of ADL leads to a significant decrease in mechanical strengths. This phenomenon is explained by the increase in the air voids inside the material and the weak ADL−cement matrix interfacial bonding. It is reported that it is required to change the surface of the fibers to improve the strength and ductility of the composites.[42]

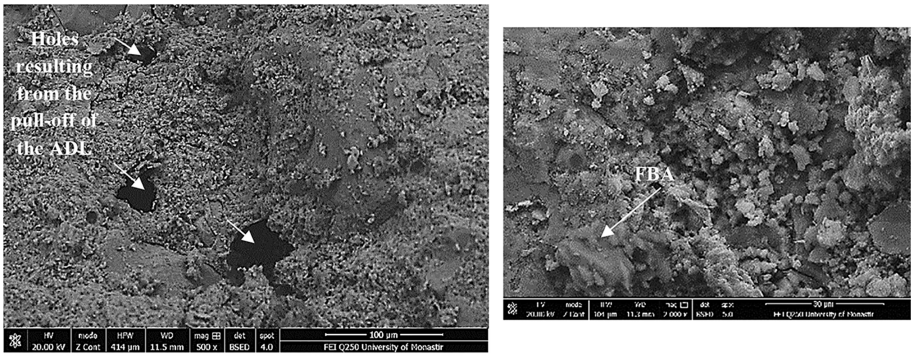

Figure 15. SEM images of the 20FBA/0.4ADL composite at (a) 100 μm and (b) 30 μm.

https://doi.org/10.1021/acsomega.2c07818
ACS Omega 2023, 8, 12039−12051

4. CONCLUSIONS

The present paper presents an experimental study that evaluates the feasibility of using FBA waste mixed with natural ADL fibers as cement mortar replacement. A preliminary characterization of FBA and ADL fibers was performed. Composites were prepared at different FBA and ADL contents. Then, their thermo-physical and mechanical properties were evaluated. The energy gain and the CO_2 emissions were also assessed. The major obtained results are as follows:

- The quality and the quantity of FBA utilized deal with both thermal and mechanical characteristics.
- Thermal conductivity measurements demonstrate that the replacement of cement by FBA enhances the thermal resistance of the composite. Thus, the proposed bio-composites can play a significant role in building thermal insulation.
- Compared to the reference mortar CM, CO_2 emissions slightly decreased thanks to the partial replacement of cement with FBA. Accordingly, the use of FBA solves the issue of waste management, protects natural resources, and reduces CO_2 emissions during cement production.
- The significant porosity of the material, poor adhesion between the fiber and mortar matrix, and the significant water uptake of ADL are the main reasons that contribute to the decrease of mechanical strength when ADL natural fibers are loaded in the cement matrix.
- The sample plasticity is improved as ADL weight fraction increases, and the breaking load of the composite material is significantly decreased.

In conclusion, the use of FBA as cement substitution should be promoted considering the improvement of insulating qualities and the decrease of environmental pollution. In the future, additional research is required, to achieve optimal mechanical and insulating properties. Further experiments of ADL ranging between 0 and 1 wt % are required in future research.

AUTHOR INFORMATION

Corresponding Author

Houda Hachem − *Research and Technology Centre of Energy (CRTEn), Hammam Lif 2050, Tunisia;* orcid.org/0000-0003-2534-0629; Email: Houda.Hachem@crten.mesrs.tn

Authors

Insaf Mehrez − *National Engineering School of Monastir (ENIM), LESTE Laboratory, University of Monastir, 5019 Monastir, Tunisia*

Ibtissem Boumnijel − *Research and Technology Centre of Energy (CRTEn), Hammam Lif 2050, Tunisia*

Abdelmajid Jemni − *National Engineering School of Monastir (ENIM), LESTE Laboratory, University of Monastir, 5019 Monastir, Tunisia*

Daoued Mihoubi − *Research and Technology Centre of Energy (CRTEn), Hammam Lif 2050, Tunisia*

Complete contact information is available at: https://pubs.acs.org/10.1021/acsomega.2c07818

Funding

The authors declare that no funds, grants, or other supports were received during the preparation of this manuscript.

Notes

The authors declare no competing financial interest.

ACKNOWLEDGMENTS

The authors acknowledge Professor Hassen Abdallah, at the Energy Research and Technology Center (CRTEn, Hammam-Lif, Tunisia), for providing the microscope and the binocular magnifier used to perform the observation.

NOMENCLATURE

A	across section(mm^2)
b	the width of test sample (m)
CI	the crystallinity index (%)
$CO_{2calcination}$	the emitted CO_2 from calcination
$CO_{2thermal\ energy\ use}$	the emitted CO_2 from the thermal energy used in the cement production
$CO_{2transportation}$	the CO_2 emissions associated with cement and clinker transportation at a certain distance by a certain mode
CO_{2tot}	total CO_2 emissions
d	distance for transportation (km)
e	the composite thickness (mm)
Eg	energy gain (%)
F	the average applied force to a cross section (N)
ft	transportation factor dependent on transportation mode
h	the thickness of the test sample in the direction of bending (m)
l	support span (0,1 m)
$I_{18°}$	the lowest intensity of the peak at about $2\theta = 18°$
$I_{22°}$	the maximum intensity of crystalline portion in the cellulose sample at about $2\theta = 22°$.
k	thermal conductivity (W m^{-1} K^{-1})
m_c	amount of cement (kg)
$p_{clinker}$	percentage of clinker in cement (%)
R	electric resistance (Ω)
R_c	the compressive strength (MPa)
R_f	the flexural strength (MPa)
S	sample surface (m^2)
t	time (s)
T_c	cold temperature (°)
T_h	hot temperature (°)
T_a	ambient temperature (°)
T_b	temperature inside the box (°)
U	tension (V)
U_{CO2}	CO_2 emitted per kg used fuel
V_{fuel}	liter of fuel (L)
W_a	water uptake (%)
w_t	weight of the sample at a time t
w_d	initial weight of the sample

Greek symbols

β thermal correction coefficient (W K^{-1})

Subscripts

ref reference material
comp proposed composite material

Abbreviations

ADL *Arundo donax* leaves
BA bottom ash
CM cement mortar

https://doi.org/10.1021/acsomega.2c07818
ACS Omega 2023, 8, 12039−12051

FA fly ash
FBA fly bottom ash
SEM scanning electron microscopy
XRD X-ray diffraction

REFERENCES

(1) Majolagbe, A. O.; Yusuf, K. A.; Agunbiade, S. E.; Oguntan, V. T. Trace Metals Charaterisation of Environmental Media (Soils, Water and Tree Barks) Around Cement Manufacturing Area, Nigeria. *Environ. Sci. Pollut. Res. Int.* **2018**, *4*, 271−274.
(2) Yang, Z.; Tian, S.; Liu, L.; Wang, X.; Zhang, Z. Application of washed MSWI fly ash in cement composites: long-term environmental impacts. *Environ. Sci. Pollut. Res. Int.* **2018**, *25*, 12127−12138.
(3) Dwivedi, A.; Jain, M. K. Fly ash−waste management and overview: A Review. *Recent Res. Sci. Technol.* **2014**, *6*, 30.
(4) Nordin, N.; Abdullah, M. M. A. B.; Tahir, M. F. M.; Sandu, A. V.; Hussin, K. Utilization of Fly Ash Waste As Construction Material. *Int. J. Conserv. Sci.* **2016**, *7*, 161.
(5) Singh, N. B. Fly ash-based geopolymer binder: A future construction material. *Minerals* **2018**, *8*, 299.
(6) He, P.; Zhang, X.; Chen, H.; Zhang, Y. Waste-to-resource strategies for the use of circulating fluidized bed fly ash in construction materials: A mini review. *Powder Technol.* **2021**, *393*, 773−785.
(7) Sun, Y.; Lee, H. Research on properties evolution of ultrafine fly ash and cement composite. *Constr. Build. Mater.* **2020**, *261*, No. 119935.
(8) Meng, J.; Zhong, J.; Xiao, H.; Ou, J. Interfacial design of nano-TiO2 modified fly ash-cement based low carbon composites. *Constr. Build. Mater.* **2021**, *270*, No. 121470.
(9) da Luz Garcia, M.; Sousa-Coutinho, J. Strength and durability of cement with forest waste bottom ash. *Constr. Build. Mater.* **2013**, *41*, 897−910.
(10) Akinyemi, B. A.; Dai, C. Development of banana fibers and wood bottom ash modified cement mortars. *Constr. Build. Mater.* **2020**, *241*, No. 118041.
(11) Maschio; Tonello, G.; Piani, L.; Furlani, E. Fly and bottom ashes from biomass combustion as cement replacing components in mortars production: Rheological behaviour of the pastes and materials compression strength. *Chemosphere* **2011**, *85*, 666−671.
(12) Barbosa, R.; Lapa, N.; Dias, D.; Mendes, B. Concretes containing biomass ashes: Mechanical, chemical, and ecotoxic performances. *Constr. Build. Mater.* **2013**, *48*, 457−463.
(13) Mehrez, I.; Hachem, H.; Gheith, R.; Jemni, A. Valorization of Posidonia-Oceanica leaves for the building insulation sector. *J. Compos. Mater.* **2022**, *56*, 1973−1985.
(14) Ardanuy, M.; Claramunt, J.; Toledo Filho, R. D. Cellulosic fiber reinforced cement-based composites: A review of recent research. *Constr. Build. Mater.* **2015**, *79*, 115−128.
(15) Babu, S. R.; Karthikeyan, S.; Senthilkumar, P.; Koodalingam, B. Mechanical behavior on tamarind & dates seeds powder, prawn shells powder with Arundo donax L. Leaf reinforced epoxy composite. *Mater. Today: Proc.* **2020**, *33*, 3031−3036.
(16) Molari, L.; Coppolino, F. S.; Garcia, J. J. Arundo donax: A widespread plant with great potential as sustainable structural material. *Constr. Build. Mater.* **2021**, *268*, No. 121143.
(17) Barreca, F. Use of giant reed Arundo Donax L. in rural constructions. *CIGR J.* **2012**, *14*, 46−52.
(18) Zámolyi, F.; Herbig, U. Reed as building material-renaissance of vernacular techniques. In *International Symposium on Advanced Methods of Monitoring Reed Habitats*; Csaplovics, E., Schmidt, J., Eds.; Rhombos Verlag: Berlin, 2011, p. 83.
(19) Andreu-Rodriguez, J.; Medina, E.; Ferrandez-Garcia, M. T.; Ferrandez-Villena, M.; Ferrandez-Garcia, C. E.; Paredes, C.; Moreno-Caselles, J. Agricultural and industrial valorization of Arundo donax L. *Commun. Soil Sci. Plant Anal.* **2013**, *44*, 598−609.
(20) Ferrandez-García, A. A.; Ortuño, T. G.; Ferrandez-Villena, M.; Ferrandez-Garcia, A.; Ferrandez-García, M. T. Evaluation of particleboards made from giant reed (arundo donax L.) bonded with cement and potato starch. *Polymer* **2022**, *14*, 111.
(21) Ferrández-García, C. E.; Andreu-Rodríguez, J.; Ferrández-García, M. T.; Ferrández-Villena, M.; García-Ortuño, T. Panels made from giant reed bonded with non-modified starches. *BioResources* **2012**, *7*, 5904.
(22) García-Ortuño, T.; Andréu-Rodríguez, J.; Ferrández-García, M. T.; Ferrández-Villena, M.; Ferrández-García, C. E. Evaluation of the physical and mechanical properties of particleboard made from giant reed (Arundo donax L.). *BioResources* **2011**, *6*, 477−486.
(23) Shon, C. S.; Mukashev, T.; Lee, D.; Zhang, D.; Kim, J. R. Can common reed fiber become an effective construction material? Physical, mechanical, and thermal properties of mortar mixture containing common reed fiber. *Sustainability* **2019**, *11*, 903.
(24) Manniello, C.; Cillis, G.; Statuto, D.; Di Pasquale, A.; Picuno, P. Concrete Blocks Reinforced with Arundo donax Natural Fibers with Different Aspect Ratios for Application in Bioarchitecture. *Appl. Sci.* **2022**, *12*, 2167.
(25) Segal, L. G. J. M. A.; Creely, J. J.; Martin, A. E., Jr.; Conrad, C. M. An empirical method for estimating the degree of crystallinity of native cellulose using the X-ray diffractometer. *Text. Res. J.* **1959**, *29*, 786−794.
(26) Mehrez, I.; Hachem, H.; Jemni, A. Thermal insulation potential of wood-cereal straws/plaster composite. *Case Stud. Constr. Mater.* **2022**, *17*, 1353.
(27) Asadi, I.; Shafigh, P.; Hassan, Z. F. B. A.; Mahyuddin, N. B. Thermal conductivity of concrete−A review. *J. Build. Eng.* **2018**, *20*, 81−93.
(28) Mounir, S.; Maaloufa, Y.; Khabbazi, A. Thermal properties of the composite material clay/granular cork. *Constr. Build. Mater.* **2014**, *70*, 183−190.
(29) Ali, M. B.; Saidur, R.; Hossain, M. S. A review on emission analysis in cement industries. *Renew. Sustainable Energy Rev.* **2011**, *15*, 2252−2261.
(30) Pommer, K.; Pade, C. *Guidelines - uptake of carbon dioxide in the life cycle inventory of concrete*; Danish Technological Institute; 2005. Web accessed at http://www.dti.dk on April 16, 2008.
(31) Anbalagan, G.; Prabakaran, A. R.; Gunasekaran, S. Spectroscopic characterization of Indian standard sand. *J. Appl. Spectrosc.* **2010**, *77*, 86−94.
(32) Hall, C. Barrier performance of concrete: a review of fluid transport theory. *Mater. Struct.* **1994**, *27*, 291−306.
(33) Olmeda, J.; De Rojas, M. S.; Frías, M.; Donatello, S.; Cheeseman, C. R. Effect of petroleum (pet) coke addition on the density and thermal conductivity of cement pastes and mortars. *Fuel* **2013**, *107*, 138−146.
(34) Caprai, V.; Gauvin, F.; Schollbach, K.; Brouwers, H. J. H. MSWI bottom ash as binder replacement in wood cement composites. *Constr. Build. Mater.* **2019**, *196*, 672−680.
(35) Demirbog, R. Thermal conductivity and compressive strength of concrete incorporation with mineral admixtures. *Build. Environ.* **2007**, *42*, 2467−2471.
(36) Demirbog, R. Influence of mineral admixtures on thermal conductivity and compressive strength of mortar. *Energy Build.* **2003**, *35*, 189−192.
(37) ASTM Standard. Standard test methods for flexural properties of unreinforced and reinforced plastics and electrical insulating materials. ASTM D790. *Annual book of ASTM standards*; ASTM, 1997.
(38) Saghrouni, Z.; Baillis, D.; Jemni, A. Composites based on Juncus maritimus fibers for building insulation. *Cem. Concr. Compos.* **2020**, *106*, No. 103474.
(39) Antiohos, S.; Maganari, K.; Tsimas, S. Evaluation of blends of high and low calcium fly ashes for use as supplementary cementing materials. *Cem. Concr. Compos.* **2005**, *27*, 349−356.
(40) Kosmatka, S. H.; Panarese, W. C.; Kerkhoff, B. *Design and control of concrete mixtures*. Portland Cement Association: Skokie, IL, 2002; pp. 60077−1083.

https://doi.org/10.1021/acsomega.2c07818
ACS Omega 2023, 8, 12039−12051

(41) Fiore, V.; Piperopoulos, E.; Calabrese, L. Assessment of Arundo donax fibers for oil spill recovery applications. *Fibers* **2019**, *7*, 75.
(42) Mehrez, I.; Hachem, H.; Gheith, R.; Jemni, A. Effect of the incorporation of NaOH-treated wood aggregates on thermal and mechanical properties of plaster mortar. *Eur. J. Wood Wood Prod.* **2023**, *81*, 411−420.
(43) Martínez-Sanz, M.; Erboz, E.; Fontes, C.; López-Rubio, A. Valorization of Arundo donax for the production of high performance lignocellulosic films. *Carbohydr. Polym.* **2018**, *199*, 276−285.
(44) Fiore, V.; Scalici, T.; Valenza, A. Characterization of a new natural fiber from Arundo donax L. as potential reinforcement of polymer composites. *Carbohydr. Polym.* **2014**, *106*, 77−83.
(45) Mehrez, I.; Hachem, H.; Gheith, R.; Jemni, A. Optimization of Mortar/Agave americana Fibers Composite Behavior Based on Experimental Design. *J. Nat. Fibers* **2023**, *20*, No. 2152149.
(46) Dodoo, A.; Gustavsson, L.; Sathre, R. Carbon implications of end-of-life management of building materials. *Resour., Conserv. Recycl.* **2009**, *53*, 276−286.
(47) Ibeto, C. N.; Obiefuna, C. J.; Ugwu, K. E. Environmental effects of concretes produced from partial replacement of cement and sand with coal ash. *Int. J. Environ. Sci. Technol.* **2020**, *17*, 2967−2976.
(48) Hamdaoui, O.; Limam, O.; Ibos, L.; Mazioud, A. Thermal and mechanical properties of hardened cement paste reinforced with Posidonia-Oceanica natural fibers. *Constr. Build. Mater.* **2021**, *269*, No. 121339.
(49) Sedan, D.; Pagnoux, C.; Smith, A.; Chotard, T. Mechanical properties of hemp fibre reinforced cement: Influence of the fibre/matrix interaction. *J. Eur. Ceram. Soc.* **2008**, *28*, 183−192.
(50) Coutts, R. S. P. Flax fibres as reinforcement in cement mortars. *Int. J. Cem. Compos. Lightweight Concr.* **1983**, *5*, 257.
(51) Bilba, K.; Arsene, M. A.; Ouensanga, A. Sugar cane bagasse fibre reinforced cement composites. Part I. Influence of the botanical components of bagasse on the setting of bagasse/cement composite. *Cem. Concr. Compos.* **2003**, *25*, 91−96.
(52) Cook, D. J.; Pama, R. P.; Weerasingle, H. L. S. D. Coir Fibre Reinforced Cement as a Low Cost Roofing Material. *Build. Sci.* **1978**, *13*, 193−198.
(53) Savastano, H., Jr.; Warden, P. G.; Coutts, R. S. P. Mechanically pulped sisal as reinforcement in cementitious matrices. *Cem. Concr. Compos.* **2003**, *25*, 311−319.
(54) Song, F. V.; Yang, B.; Di Tommaso, D.; Donnan, R. S.; Chass, G. A.; Yada, R. Y.; Tian, K. V. Resolving nanoscopic structuring and interfacial THz dynamics in setting cements. *Mater. Adv.* **2022**, *3*, 4982−4990.
(55) Liu, P.; Feng, C.; Wang, F.; Gao, Y.; Yang, J.; Zhang, W.; Yang, L. Hydrophobic and water-resisting behavior of Portland cement incorporated by oleic acid modified fly ash. *Mater. Struct.* **2018**, *51*, 38.

https://doi.org/10.1021/acsomega.2c07818
ACS Omega 2023, 8, 12039−12051